Supplementary Information for

TMAO mediates effective attraction between lipid membranes by partitioning unevenly between bulk and lipid domains

Shahar Sukenik[a,b], Shaked Dunsky[a], Avishai Barnoy[a], Ilan Shumilin[a], and Daniel Harries[a,*]

[a]Institute of Chemistry and the Fritz Haber Research Center, The Hebrew University, Jerusalem 91904, Israel.
[b]Current address: Department of Chemistry, School of Chemical Sciences, University of Illinois at Urbana−Champaign, Urbana, Illinois 61801, United States.
[*]Corresponding author. Email: daniel@fh.huji.ac.il

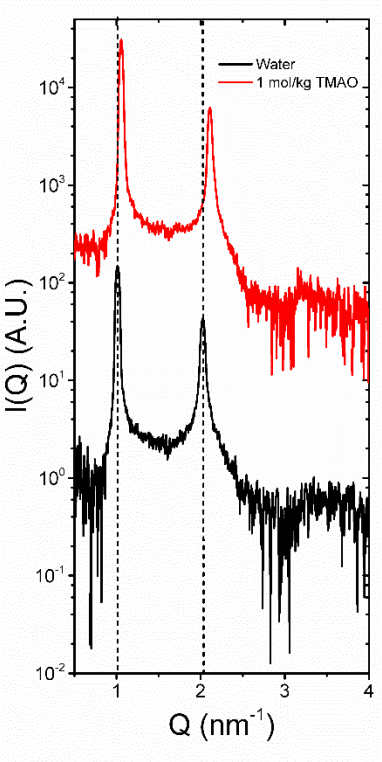

Figure S1 | Radially integrated small angle X-ray scattering intensity versus scattering wave vector in the absence (black) and presence (red) of 1 mol/kg TMAO. Vertical dashed lines represent the peak position for water, highlighting the shift between DMPC in water and in 1 mol/kg TMAO.

Table S1. Details of simulation setups: number of molecules and duration

	0 m	0.1 m	0.5 m	1 m
Water	4753	4668	4710	4668
TMAO	0	9	42	84
DMPC	128	128	128	128
t (ns)	100	100	100	100

Table S2. Membrane bilayer physical constants for different TMAO concentrations derived from MD simulations

	Property description	0 m	0.1 M	0.5 m	1 m
D'_B [Å] [a]	Bilayer thickness	35.7 ± 0.2	36 ± 1	35.9 ± 0.2	36.6 ± 0.2
A_L [Å^2] [a]	Area per lipid	60.8 ± 0.4	60.3 ± 0.4	60.3 ± 0.4	57.75 ± 0.35
PN [°]	Average headgroup dipole orientation	69.96	70.14	70.71	71.26
K_c [kT] [b]	Monolayer Bending modulus	6.9 ± 0.4	6.8 ± 0.2	7.4 ± 0.6	7.7 ± 0.4
ξ_0 [Å] [c]	Water spatial correlation decay length	1.46 ± 0.05	1.56 ± 0.03	1.52 ± 0.06	1.45 ± 0.06

a. Error was obtained using the block averaging method.(14)
b. Error represents s.d. when choosing different sub-segments for analysis, and different ranges for the quadratic fit as in ref (15)
c. In order to compare the water decay length at the different TMAO concentrations from simulations, we fit the decays shown in **Fig. 2c** to the functional form taken from Marčelja and Radić(16), following an analysis similar to that presented in Schneck et al.:(17)

$$\langle \cos\delta \rangle_Z = \langle \cos\delta \rangle_{Z=-D'_w/2} \frac{\sinh\left(\xi_0^{-1} Z\right)}{\sinh\left(\xi_0^{-1} D'_w/2\right)} . \qquad \text{(S1)}$$

Here, the order parameter $\langle \cos\delta \rangle_z$ is the average dipole orientation of the water relative to the membrane normal at distance Z to the solvent midplane, and the fit was performed up to (but not into) the headgroup region. Error is determined by the fit's 95% confidence bounds. See also **Fig. 2c**.

S1. Membrane thickness determination using the gravimetric method.

To calculate the Gibbs-Luzzati bilayer thickness, D_B, (shown schematically in **Fig. 1b**) swelling curves were obtained by adding solutions of known composition and weight to lipid of known weight, determined gravimetrically.(18, 19) Samples were equilibrated, and *D* spacing determined using SAXS, as described in **SI Appendix Section S2.** The curves of *D* vs. $1/\phi_L$ show saturation at the point where bilayer repeat spacing D no longer changes with lipid volume fraction, ϕ_L (indicated by the vertical dashed lines shown in **Fig. 2a** and **b**). At this first point of full hydration the relation $D = \phi_L D_B$ exactly holds. The error in D_B (shown in Fig. 2) is calculated from the intersection between the fully hydrated lipid and the limits of the 95% confidence bands of the linear fit. The lipid volume fraction, ϕ_L, is given by

$$\phi_L = \left[1 + \frac{n_{sol}\bar{v}_{sol}}{n_L \bar{v}_L} \right]^{-1}. \qquad \text{(S2)}$$

Where n_i is the number of moles of species *i*, and $\bar{v}_i$ is the specific volume of the component. In **Eq. S2**, subscript L denotes the lipid component ($\bar{v}_L = 0.978$ ml/g for DMPC (20)) and sol denotes the solution included between bilayers. The number of moles are calculated from weights obtained using a Mettler Toledo Excellence Plus XP microbalance.

S2. Determination of inter-bilayer solvent thickness D'_w

To calculate the inter-bilayer solvent thickness, we rely on lipid incompressibility and use the volume per DMPC molecule, $V_L =$ 1,100 Å^3, to calculate the lipid bilayer thickness as $D_B = 2V_L/A_L$, where A_L is the surface area per lipid. We use the data from Kinnun et al.(21) to evaluate the area per lipid as a function of applied pressure, and find a minor change only at very high exerted pressures. Using the bilayer thickness, we find the water layer thickness through $D_w = D - D_B$. We moreover find an exact overlap between our data of osmotic stress curves (shown as blue squares in **Fig. 3a**) and D'_w as reported by Nagle et al(20) by subtracting a constant 6.05 Å from our D_w data (in the absence of TMAO), so that $D'_w = D - D_B - 6.05\text{Å}$.

Table S3. Parameters used for EOS fitting

symbol	meaning	value
H [a,b]	Hamaker constant	4.88×10^{-14} erg
P_H	Hydration force amplitude	1.13×10^{9} dyn/cm^2
λ [b]	Hydration force decay length	1.97 Å
K_c [b,c]	Bilayer rigidity	8×10^{-13} erg
A_0 [d]	Amplitude of membrane fluctuations	1.09 Å^{-2}
λ_{fl} [d]	Membrane fluctuation decay length	5.1 Å

a. value is given for pure DMPC in water (no TMAO). Values for TMAO solutions are calculated as described in **section S5**.
b. Values taken from ref. (22)
c. Value is varied in **Fig. 3b** to see the limits of bilayer rigidity effect
d. Values derived from the fit of the mean square fluctuation of lipid bilayer with respect to the water spacing, following the data and analysis in ref. (22). See **section S6** for details.

S3. Calculation of Hamaker constant

Using Lifshitz theory it is possible to derive the value of the Hamaker constant, as long as the dielectric permittivity of the media and its variation with frequency are known. We consider the case of two identical (say lipid, *L*) phases interacting across another medium (say aqueous solution, *sol*), where the expression for the Hamaker constant is(23, 24)

$$H = \frac{3}{4} kT \left(\frac{\varepsilon_L - \varepsilon_{sol}}{\varepsilon_L + \varepsilon_{sol}} \right)^2 + \frac{3h\nu_e}{16\sqrt{2}} \frac{\left(\zeta_L^2 - \zeta_{sol}^2 \right)^2}{\left(\zeta_L^2 + \zeta_{sol}^2 \right)^{3/2}} \tag{S4}$$

In this expression ε_i is the dielectric constant, ζ_i is the refractive index of the medium at visible wavelength, ν_e is the main electronic absorption frequency in the UV, $\approx 3 \times 10^{15} s^{-1}$. Accordingly, we have used $h\nu = 2 \times 10^{-18}$ J. We also use available experimentally derived values of the spectroscopic parameters. The refractive index of TMAO solutions at a given concentration was evaluated from the experimentally determined expression (25, 26)

$$c_{TMAO} = -0.0038 + 103.3151 \times \Delta\zeta - 259.43 \times \Delta\zeta^2 , \tag{S5}$$

where $\Delta\zeta = \zeta_{water} - \zeta_{sol}$, and the index of refraction of water at 30°C is $\zeta_{water} = 1.3313$.(27) The dielectric permittivity of TMAO solutions were taken from ref. (28) by using the relation $\varepsilon_{sol} = 76.5 + 5c_{TMAO}$, which properly interpolates values from no TMAO at 30 °C to the highest concentrations we have used in this study. The dielectric permittivity of the lipid (hydrocarbon) part was assumed to be 2 throughout.(23, 24) The values in pure water as solvent derived from **Eq. S4** correspond to Hamaker constants determined also in other models of lipids, including in the modeling of the high resolution x-ray study of Petrache et al(22). Overall, the presence of TMAO acts to reduce the Hamaker constant, as shown in **Fig. S2**, indicating a weakening of the vdW attraction between membranes. We have compared the results from this model with those of a more elaborate model(29) that contains an additional slab of TMAO-free solvent close to the membrane interface that would correspond to the

volume of TMAO exclusion. The results for this model deviate significantly from those of the more simple model described here only at very high TMAO concentrations, above 2m, which we did not attempt to model in this work. Importantly, the estimated Hamaker coefficient will not change the fundamental conclusions we have reached. For example, even reducing the change in the Hamaker constant from the value in pure water due to TMAO by 50% would only change K_P (see **Fig. 4**) by ± 0.0001 at 1m concentration, and the conclusion that K_P <1 will remain the same for all concentrations.

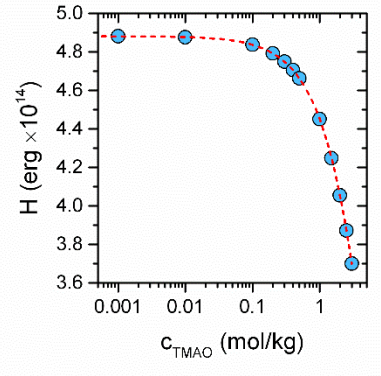

Figure S2 | Hamaker constants derived for various concentrations of TMAO. Red line guide to the eye is a quadratic fit of the calculated data points.

S4. Calculation of the derivative of the mean square fluctuation of the membrane

The last term in the EOS (**Eq. 1**) requires the derivative of the membrane fluctuations with respect to D'_w .The values for these fluctuations has been obtained from high resolution X-ray scattering experiments of DMPC at 30°C, as reported in Petrache et al.(22) We used the data from Fig. 5a in ref. (22) and following the procedure in work, we fit σ^{-2} vs D'_w, to an exponential function, so that

$$\frac{d\sigma^{-2}}{dD'_w} = -\frac{A_0}{\lambda_{fl}} e^{\frac{-D'_w}{\lambda_{fl}}} . \qquad \text{(S3)}$$

Fitting according to ref. (22) results in A_0 =1.09 Å^{-2} and λ_{fl} = 5.1 Å.

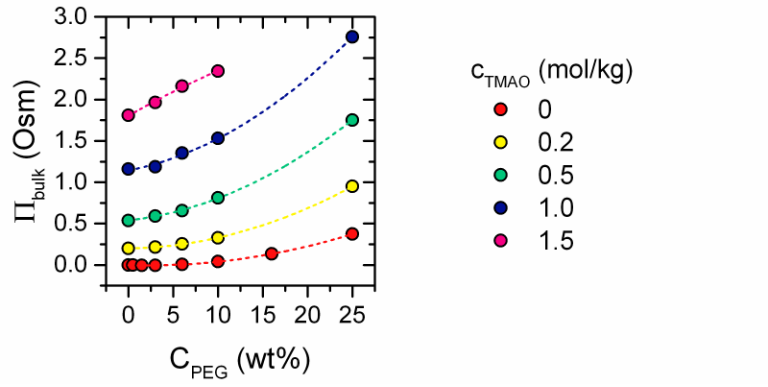

Figure S3 | Measured osmotic pressure of water:PEG:TMAO tertiary solutions. Data for PEG solution in the absence of TMAO is taken from P. Rand.(30) Colors represent TMAO concentrations. Dashed lines are guides for the eye. We find that the rise in measured TMAO osmotic pressure in the presence of PEG can be explained by uptake of water molecules by PEG that are essentially inaccessible to TMAO, an effect that has not been addressed previously.

S5. Calculation of TMAO preferential interaction coefficient with membrane from simulations

The thermodynamic property that is relevant for determining the lipid preferential hydration in TMAO solutions is Γ_w, the preferential interaction coefficient. The parameter Γ_w expresses the net number of water molecules from which TMAO is excluded per lipid. A positive Γ_w value describes TMAO exclusion from the membrane, and a negative Γ value describes a preferential inclusion of TMAO in the membrane domain. To extract Γ_w from the simulation we use $\Gamma_w(Z)$, defined as (31)

$$\Gamma_w(Z) = N_W\left(1-\frac{N_T/N_W}{n_T/n_W}\right). \qquad \text{(S3)}$$

In this definition, we divide the aqueous medium into two domains (or "slabs"): the membrane slab (from bilayer to Z), and the bulk layer (from Z to water's midplane). In **Eq. 1**, N_W and N_T represent the number of water and TMAO molecules in the membrane slab (per lipid), and n_W and n_T represent the number of water and TMAO molecules in the bulk layer, respectively. The value at which $\Gamma_w(Z)$ converges, as shown in **Fig. S4,** is the preferential hydration coefficient Γ_w. The value of Γ_w may also be calculated using the alternative, yet completely equivalent, Kirkwood-Buff approach.(32) Calculating Γ_w by both methods yielded similar results indicating that $\Gamma_w \approx 11$ water molecules from which TMAO is excluded for all TMAO concentrations simulated, **Fig. S4** and inset of **Fig. 5a**.

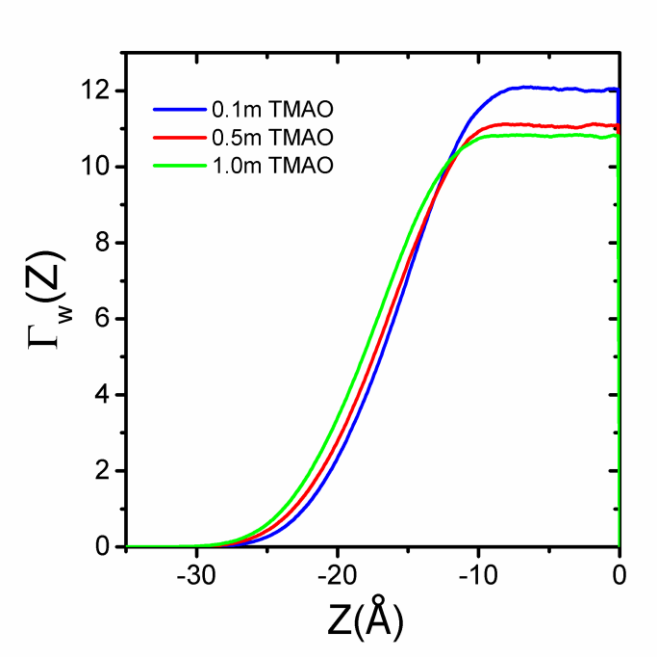

Figure S4 | The cumulative preferential hydration, $\Gamma_w(Z)$ at three TMAO concentrations. The number of TMAO-excluding waters per lipid, $\Gamma_w \approx 11$, as seen by the convergence towards the bulk.

S6. Addition of high pressure term to EOS

We found that is not possible to describe our experimental curves at high TMAO concentrations and high PEG exerted pressure with the EOS in **Eq. 1**, due to an upward inflection in the isotherms at these concentrations, **Fig. S5a**. Specifically, the data indicates that in this range there is a strong TMAO concentration dependent repulsion between the bilayers that cannot be accounted for using the usual hydration interaction. This repulsion has a very short decay length and an amplitude that grows steeply with TMAO concentration. To account for this additional component, we can add a corresponding phenomenological term to **Eq. 1**, which then becomes,

$$\Pi_{EOS} = -\frac{H}{6\pi}\frac{1}{D_w'^3} + P_h e^{-\frac{D_w'}{\lambda}} + \left(\frac{k_B T}{2\pi}\right)^2 \frac{1}{K_c}\frac{a_0}{\lambda_{fl}} e^{-\frac{D_w'}{\lambda_{fl}}} + P_t e^{-\frac{D_w'}{\lambda_t}}, \qquad \text{(S5)}$$

with P_t describing the amplitude and λ_t denoting the decay length of this additional force. We fit this equation to our high TMAO concentration curves ($c_{TMAO} \geq 0.5$ mol/kg) and find an excellent match with our experiments when λ_t = 0.5 Å for all curves, as shown for the high-pressure region in **Fig. S5b**. We suggest that this term may represent the solvation force that residual TMAO exerts when membranes come within a few angstroms of each other. Because TMAO is significantly larger than water, these forces are experienced at distances larger than those at which hydration forces become strongest. Although we found no evidence for lipid phase transitions in the wide angle SAXS regime (e.g. to the gel phase) under these high PEG pressure conditions, we cannot completely exclude the possibility that under these extreme osmotic pressures and high TMAO concentrations there are additional structural changes to the lipid bilayer that would change its apparent thickness.

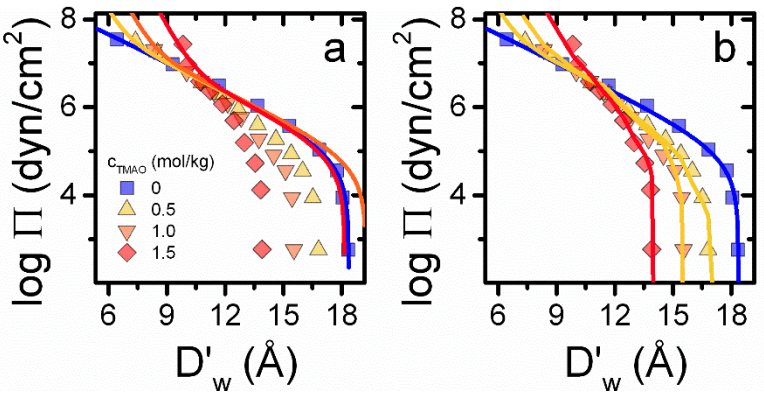

Figure S5 | Fourth term in EOS required to fit experimental data at high pressures. Symbols are experimental data points and lines are the EOS. Water curve (blue) is shown for reference. (**a**) Without the addition of the fourth term (**Eq. S5**), all EOS lines would coincide with water at high pressures. The strong deviation above log P > 6 indicates the presence of an additional force. At lower pressures, however, the fit is poor. This is because the excess pressure exerted by uneven partitioning of TMAO is not accounted for. (**b**) Subtracting the pressure inside the lipid bilayers, Π_{MLV}, from the EOS curves (see main text), the isotherms overlap our experimental results over the entire experimental range.

References

1. Russo AT, Rösgen J, Bolen DW (2003) Osmolyte Effects on Kinetics of FKBP12 C22A Folding Coupled with Prolyl Isomerization. *J Mol Biol* 330(4):851–866.
2. Petrache HI, Harries D, Parsegian VA (2007) Measurement of Lipid Forces by X-Ray Diffraction and Osmotic Stress. *Methods in Molecular Biology*, pp 405–419.
3. Nadler M, et al. (2011) Following the structural changes during zinc-induced crystallization of charged membranes using time-resolved solution X-ray scattering. *Soft Matter* 7(4):1512–1523.
4. Hammersley A (1997) FIT2D: an introduction and overview. *European Synchrotron Radiation Facility Internal Report ESRF97HA02T*, pp 1–33.
5. Ben-Nun T, Ginsburg A, Székely P, Raviv U (2010) X+: a comprehensive computationally accelerated structure analysis tool for solution X-ray scattering from supramolecular self-assemblies. *J Appl Crystallogr* 43(6):1522–1531.
6. Wu EL, et al. (2014) CHARMM-GUI membrane builder toward realistic biological membrane simulations. *J Comput Chem* 35(27):1997–2004.
7. Huang J, Mackerell AD (2013) CHARMM36 all-atom additive protein force field: Validation based on comparison to NMR data. *J Comput Chem* 34(25):2135–45.
8. Jorgensen WL, Chandrasekhar J, Madura JD, Impey RW, Klein ML (1983) Comparison of simple potential functions for simulating liquid water. *J Chem Phys* 79(2):926–935.
9. Vanommeslaeghe K, et al. (2009) CHARMM general force field: A force field for drug-like molecules compatible with the CHARMM all-atom additive biological force fields. *J Comput Chem* 31(16):NA-NA.
10. Phillips JC, et al. (2005) Scalable molecular dynamics with NAMD. *J Comput Chem* 26(16):1781–1802.

11. Nosé S, Klein ML (1983) Constant pressure molecular dynamics for molecular systems. *Mol Phys* 50(5):1055–1076.

12. Essmann U, et al. (1995) A smooth particle mesh Ewald method. *J Chem Phys* 103(November):8577–8593.

13. Humphrey W, Dalke A, Schulten K (1996) VMD: visual molecular dynamics. *J Mol Graph Model* 14(1):33–38.

14. Grossfield A, Zuckerman DM (2009) Quantifying uncertainty and sampling quality in biomolecular simulations. *Annu Rep Comput Chem* 5(9):23–48.

15. Khelashvili G, Kollmitzer B, Heftberger P, Pabst G, Harries D (2013) Calculating the bending modulus for multicomponent lipid membranes in different thermodynamic phases. *J Chem Theory Comput* 9(9):3866–3871.

16. Marčelja S, Radić N (1976) Repulsion of interfaces due to boundary water. *Chem Phys Lett* 3(1):129–130.

17. Schneck E, Sedlmeier F, Netz RR (2012) Hydration repulsion between biomembranes results from an interplay of dehydration and depolarization. *Proc Natl Acad Sci* 109(36):14405–14409.

18. Aroti A, Leontidis E, Dubois M, Zemb T (2007) Effects of monovalent anions of the hofmeister series on DPPC lipid bilayers Part I: swelling and in-plane equations of state. *Biophys J* 93(5):1580–90.

19. Tristram-Nagle S (2015) Use of x-ray and neutron scattering methods with volume measurements to determine lipid bilayer structure and number of water molecules/lipid. *Subcell Biochem* 71:17–43.

20. Nagle JF, Tristram-Nagle S (2000) Structure of lipid bilayers. *Biochim Biophys Acta* 1469(3):159–195.

21. Kinnun JJ, Mallikarjunaiah KJ, Petrache HI, Brown MF (2015) Elastic deformation and area per lipid of membranes: Atomistic view from solid-state deuterium NMR spectroscopy. *Biochim Biophys Acta - Biomembr* 1848(1):246–259.

22. Petrache HI, et al. (1998) Interbilayer interactions from high-resolution x-ray scattering. *Phys Rev E* 57(6):7014–7024.

23. Parsegian VA (2005) *Van der Waals Forces* (Cambridge University Press, Cambridge) doi:10.1017/CBO9780511614606.

24. Israelachvili JN (2011) *Intermolecular and surface forces* (Academic Press).

25. Baskakov I, Wang A, Bolen DW (1998) Trimethylamine-N-Oxide Counteracts Urea Effects on Rabbit Muscle Lactate Dehydrogenase Function: A Test of the Counteraction Hypothesis. *Biophys J* 74(5):2666–2673.

26. Wang AJ, Bolen DW (1997) A naturally occurring protective system in urea-rich cells: Mechanism of osmolyte protection of proteins against urea denaturation. *Biochemistry* 36(30):9101–9108.

27. Lide DR (2009) *CRC Handbook of Chemistry and Physics* doi:10.1021/ja906434c.

28. Hunger J, Ottosson N, Mazur K, Bonn M, Bakker HJ (2015) Water-Mediated Interactions between Trimethylamine-N-Oxide and Urea. *Phys Chem Chem Phys* 17(1):298–306.

29. LeNeveu DM, Rand RP (1977) Measurement and modification of forces between lecithin bilayers. *Biophys J* 18(2):209–30.

30. Rand RP Osmotic Pressure Data. Available at: https://brocku.ca/researchers/peter_rand/osmotic/osfile.html#data [Accessed March 7, 2017].

31. Ghosh T, Kalra A, Garde S (2005) On the salt-induced stabilization of pair and many-body hydrophobic interactions. *J Phys Chem B* 109(1):642–51.

32. Harries D, Rosgen J (2008) A practical guide on how osmolytes modulate macromolecular properties. *Methods Cell Biol* 84(7):679–735.